Biophysical *Journal*
Article

Biophysical Society

Age-related degradation of tectorial membrane dynamics with loss of CEACAM16

Amer Mansour,[1] Jonathan B. Sellon,[1] Daniel Filizzola,[1] Roozbeh Ghaffari,[1] Mary Ann Cheatham,[2] and Dennis M. Freeman[1,3,*]

[1]Research Laboratory of Electronics, Massachusetts Institute of Technology, Cambridge, Massachusetts; [2]Roxelyn and Richard Pepper Department of Communication Sciences and Disorders, Knowles Hearing Center, Northwestern University, Evanston, Illinois; and [3]Department of Electrical Engineering and Computer Science, Massachusetts Institute of Technology, Cambridge, Massachusetts

ABSTRACT Studies of genetic disorders of sensorineural hearing loss have been instrumental in delineating mechanisms that underlie the remarkable sensitivity and selectivity that are hallmarks of mammalian hearing. For example, genetic modifications of TECTA and TECTB, which are principal proteins that comprise the tectorial membrane (TM), have been shown to alter auditory thresholds and frequency tuning in ways that can be understood in terms of changes in the mechanical properties of the TM. Here, we investigate effects of genetic modification targeting CEACAM16, a third important TM protein. Loss of CEACAM16 has been recently shown to lead to progressive reductions in sensitivity. Whereas age-related hearing losses have previously been linked to changes in sensory receptor cells, the role of the TM in progressive hearing loss is largely unknown. Here, we show that TM stiffness and viscosity are significantly reduced in adult mice that lack functional CEACAM16 relative to age-matched wild-type controls. By contrast, these same mechanical properties of TMs from juvenile mice that lack functional CEACAM16 are more similar to those of wild-type mice. Thus, changes in hearing phenotype align with changes in TM material properties and can be understood in terms of the same TM wave properties that were previously used to characterize modifications of TECTA and TECTB. These results demonstrate that CEACAM16 is essential for maintaining TM mechanical and wave properties, which in turn are necessary for sustaining the remarkable sensitivity and selectivity of mammalian hearing with increasing age.

SIGNIFICANCE The tectorial membrane (TM) is required for mechanical stimulation of cochlear sensory receptors and thus plays an essential role in controlling the remarkable sensitivity and frequency selectivity of mammalian hearing. Although progressive losses of sensitivity and selectivity have been linked to changes in sensory receptor cells, modifications in TM properties and their role in progressive hearing loss remain largely unknown. Recent studies have shown that loss of CEACAM16, an integral component of the TM, leads to changes in TM physical structure and progressive loss of hearing sensitivity with increasing age. Here, we show that alterations in TM mechanical properties and traveling waves in *Ceacam16*$^{\beta gal/\beta gal}$ mice contribute to progressive changes in sensitivity.

INTRODUCTION

The mammalian cochlea is a remarkable sensor that can reliably detect vibrations on the order of picometers (1), and perform high-quality frequency analysis such that the frequency of sound is mapped to place along the cochlear partition (2). Mechanical measurements have established that high sensitivity, sharp tuning, and nonlinearity are already manifest in the peripheral stages of auditory processing (3). It is now widely accepted that these remarkable properties ultimately derive from active mechanical amplification residing in the cochlea. Although there is ongoing debate about the nature of the cochlear amplifier, many observations point to somatic motility of outer hair cells (4) generated by prestin (5,6) as the principal component of the amplifier. Genetic manipulations that eliminate prestin-based somatic electromotility cause significant hearing loss (7). Hair-bundle-based adaptation mechanisms, which are important for amplifying the response to sound in non-mammalian cochleae, are also present in mammalian hair cells (8–10), suggesting that bundle-based amplification also plays a role in cochlear mechanics. In addition, genetic manipulations of proteins in the tectorial membrane (TM)

Submitted April 7, 2021, and accepted for publication September 16, 2021.

*Correspondence: freeman@mit.edu

Amer Mansour and Jonathan B. Sellon contributed equally to this work.

Editor: Jeremiah J. Zartman.

https://doi.org/10.1016/j.bpj.2021.09.029

have been shown to cause hearing loss (11–13). Recent studies suggest complex phenomena associated with the TM, such as resonance (14,15), pulsatile radial fluid flow (16), TM traveling waves (17–23), and poroelastic effects (22,24) are all linked with cochlear sensitivity and tuning. The development of mouse models of genetic hearing disorders that exclusively target the TM have linked changes in sensitivity and tuning in mutant mice with changes to the TM (11–13,25–28). The wide range of functional deficits associated with these mouse models illustrates the importance of this accessory structure to the integrity of the amplifying feedback loop in which outer hair cells' somatic and bundle motility reside. Although there has been progress in elucidating the importance of TM traveling waves in the mechanical excitation of cochlear hair cells, the mechanisms by which the dynamic mechanical properties of the TM contribute to system-level amplification and how alterations might influence age-related hearing loss remain unclear. Studies examining protein turnover in the cochlea have revealed that the TM is a relatively stable structure (29). However, recent studies have shown that loss of CEACAM16, an abundant protein that comprises the TM's striated sheet structure along with TECTA and TECTB (12,13,30–33), leads to anatomical changes and progressive decline in hearing function. Apart from the increased incidence of spontaneous otoacoustic emissions (SOAEs), cochlear function in *Ceacam16*$^{\beta gal/\beta gal}$ mutant mice is near normal in juveniles at$\sim$1 month of age. However, distortion product otoacoustic emissions (DPOAE) decrease and auditory brainstem response (ABR) thresholds increase at older ages when compared with *Ceacam16*$^{+/+}$ mice (34). By one year of age, mice lacking CEACAM16 have significantly elevated ABR thresholds at all frequencies and no emissions of any kind. These changes have been attributed to a progressive loss of matrix from the core of the TM and to accelerated age-related degeneration of the TM in *Ceacam16*$^{\beta gal/\beta gal}$ mice (28,34).

CEACAM16 has been posited to interact with TECTA and TECTB (28,34), thereby forming the TM's striated sheet matrix (33). Although transcription of *Tecta* and *Tectb* is critical for the development of TM structure (35), mRNA for these two genes is not measurable after weaning in mice (36). In contrast, *Ceacam16* is transcribed and CEACAM16 is secreted in adult mice by a variety of nonsensory and supporting cells, including epithelial cells of the spiral limbus and inner sulcus, border cells, inner and outer pillar cells, and Deiters' cells (28). Continued expression of CEACAM16 by a variety of cell types and its interaction with other TM striated sheet proteins suggests that it plays an essential role in maintaining the structure of the TM with increasing age.

To better understand how the loss of functional CEACAM16 affects cochlear mechanisms, we explore dynamic wave properties of TMs from *Ceacam16*$^{\beta gal/\beta gal}$ and *Ceacam16*$^{+/+}$ mice at various ages. We show that TM traveling wave decay constants and wave speeds, measured in isolated TM segments excised from the middle cochlear turn, are reduced in adult *Ceacam16*$^{\beta gal/\beta gal}$ mice ($\sim$12–14 weeks of age) compared with juvenile *Ceacam16*$^{\beta gal/\beta gal}$ ($\sim$4–6 weeks of age) and adult *Ceacam16*$^{+/+}$ mice. Loss of sensitivity in mice lacking CEACAM16 could therefore relate to changes in the mechanical interactions between motion patterns along the basilar membrane and TM. We analyze traveling wave properties of the TM and determine the corresponding material properties, including shear storage modulus (G') and shear viscosity (η). In addition to determining wave properties, these material properties may also have a direct effect on the stimulation of hair bundles of sensory hair cells and on the magnitudes of DPOAEs produced in these mutants.

MATERIALS AND METHODS

Isolated TM preparation

TM segments were isolated from mice ranging from 4 to 14 weeks of age using previously published techniques (37). One TM segment was isolated from each of six *Ceacam16*$^{+/+}$ mice (12–14 weeks of age), from each of two juvenile *Ceacam16*$^{\beta gal/\beta gal}$ mice (4–6 weeks of age) and from each of five adult *Ceacam16*$^{\beta gal/\beta gal}$ (12–14 weeks of age) mice. All of the TM segments were from the mid apical region of the cochlea. All of these experimental animals originated from C57Bl/6J background strains. Cochleae were surgically excised and immersed in artificial endolymph (AE) containing 174 mM KCl, 5 mM HEPES, 3 mM dextrose, 2 mM NaCl, and 0.02 mM $CaCl_2$. The AE bath was equilibrated at room temperature to pH 7.15. The bone encasing the cochlea was removed with a #11 scalpel blade to expose the Organ of Corti. Bright- and dark-field illumination using a dissection microscope (Zeiss, Oberkochen, Germany) allowed for visualization of the TM along the cochlear spiral. A sterile eyelash was then used to remove the membrane from its limbal attachment to the Organ of Corti. TM segments from the middle cochlear turn were then removed using a micropipette and placed in fresh AE in preparation for wave chamber experiments. The care and use of animals in this study were approved by the Massachusetts Institute of Technology Committee on Animal Care.

TM wave chamber

Isolated TM segments were suspended between vibrating and stationary supports in a wave chamber containing AE (Fig. 1 *A*). The vibrating support was attached to the underlying glass slide through a piezoelectric actuator (Thorlabs, Newton, NJ) that delivered sinusoidal motions in the radial direction at audio frequencies (10–20 kHz). The stationary support was attached directly to the underlying glass slide. Using a sterile eyelash, a TM segment was carefully attached to the top surfaces of the supports, which had previously been coated with 3 μL of tissue adhesive (Cell-Tak; Collaborative Research, Bedford, MA).

Optical imaging and analysis

Stop-action images of sinusoidally excited TM segments were obtained using stroboscopic illumination from a light-emitting diode that was focused on TM samples with the transmitted-light condenser (0.8 N.A.) of a light microscope (Zeiss Axioplan; Carl Zeiss, Oberkochen, Germany). The resulting images from a 20$\times$ water-immersion objective (0.5 N.A.) were captured with a five-megapixel charge-coupled device camera (Stingray; Allied Vision Technologies, Singapore, Singapore). Images were obtained

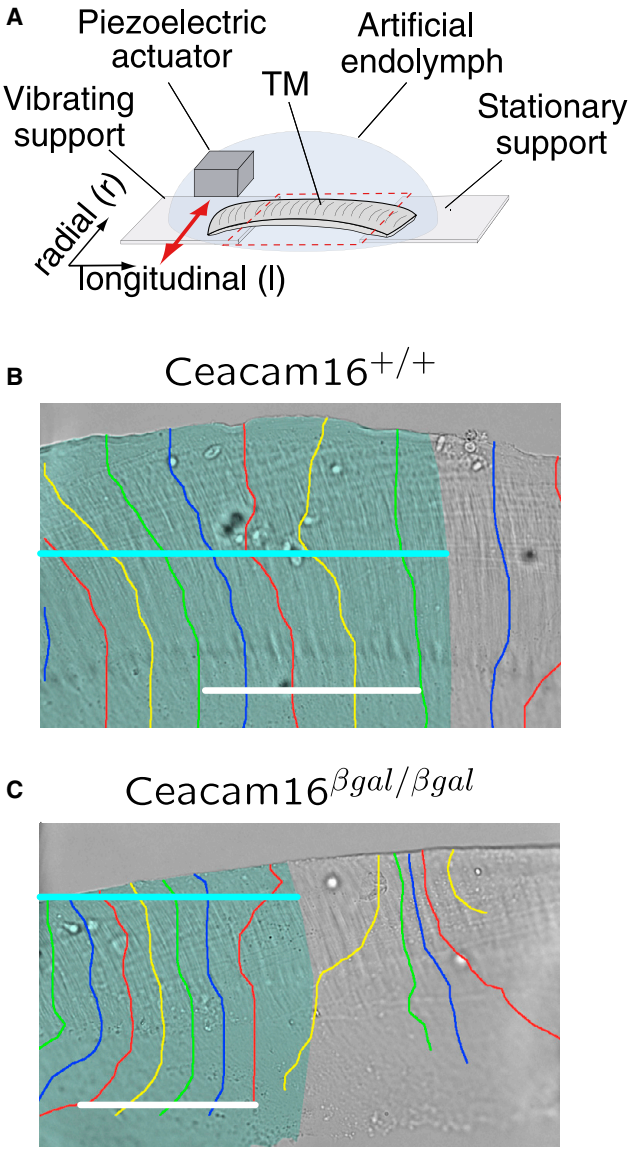

FIGURE 1 Measurement technique, analysis, and representative results. (*A*) Schematic illustration of TM wave chamber and measurement system. A segment of an isolated TM is suspended in artificial endolymph (AE) between two glass cover slips so that vibrations of the left cover slip excite radial motions of the TM that propagate as a wave traveling in the longitudinal direction. The amplitude and phase of motion as a function of pixel location is determined from stroboscopic images obtained with a video microscope at eight phases of the sinusoidal stimulus. (*B* and *C*) Representative results. Images of the TM are shaded (*cyan*) to indicate the region where the amplitude of motion is attenuated by less than a factor of e relative to the amplitude of at the edge of the vibrating support. The width of this region is given by the decay constant σ and is represented in this figure by the length of the cyan line. The smaller decay constant in (*C*) (135 μm) relative to (*B*) (221 μm) indicates less spread of excitation in the *Ceacam16*$^{\beta gal/\beta gal}$ preparation than in the wild-type preparation. The colored lines represent lines of constant phase separated by $2\pi/16$ radians, which is equal to the wavelength λ divided by 16. The smaller separation between these lines in (*C*) (95 μm) relative to those in (*B*) (116 μm) indicates that the wave in the *Ceacam16*$^{\beta gal/\beta gal}$ preparation travels more slowly (3.80 m/s) than that in the wild-type preparation (4.64 m/s). The stimulus frequency was 10 kHz. To see this figure in color, go online.

at each of eight evenly spaced phases of the sinusoidal stimulus, and motions were computed using an optical flow algorithm (38,39). The magnitudes and angles of the resulting radial TM motions at each pixel location (Fig. 1, *B* and *C*) were calculated as a function of longitudinal distance l from the vibrating support, and results were fitted using least-squares to a decaying exponential given by the real of the following expression:

$$Ae^{-jkl}, \tag{1}$$

where A is a complex-valued constant and k is a complex-valued wave number, whose real and imaginary parts determine the wavelength λ (i.e., the distance the wave travels during one period of the sinusoidal stimulation) and wave decay constant σ (i.e., the distance the wave travels as the amplitude of the motion decays by a factor of e), as shown in the following equation:

$$k = \frac{2\pi}{\lambda} - j\frac{1}{\sigma}, \tag{2}$$

where $j = \sqrt{-1}$. The speed of the traveling wave is $v = f\lambda$, where f represents the stimulation frequency in hertz.

RESULTS AND DISCUSSION

TM wave parameters for *Ceacam16*$^{\beta gal/\beta gal}$ and wild-type TMs

We measured TM wave motions in both wild-type mice (*Ceacam16*$^{+/+}$) and mice without functional CEACAM16 (*Ceacam16*$^{\beta gal/\beta gal}$). Representative results for TMs from adult mice are shown in Fig. 1, *B* and *C* and illustrate two important trends; TM waves propagate more slowly and dissipate over shorter longitudinal distances in TMs from adult *Ceacam16*$^{\beta gal/\beta gal}$ mice than in TMs from adult wild-type mice. As the TM wave propagates, the amplitude of motion tends to decrease with distance. The shaded regions of Fig. 1, *B* and *C* highlight the portions of the TM for which the amplitude of the radial motion is attenuated by less than a factor of $e \approx 2.718$ relative to that of the vibrating support. The width of this region corresponds to one decay constant σ, which is illustrated by the horizontal cyan bars in Fig. 1, *B* and *C*. The average decay constant is larger for this wild-type TM ($\sigma = 221$ μm) than it is for this *Ceacam16*$^{\beta gal/\beta gal}$ TM ($\sigma = 135\mu$m). These results suggest that mechanical spread of excitation through the TM would be smaller in *Ceacam16*$^{\beta gal/\beta gal}$ TMs than in wild-type TMs. As the TM wave propagates, the phase of motion also tends to decrease. The colored lines in Fig. 1, *B* and *C* illustrate lines of constant phase separated by $2\pi/16$ radians. Wave speed v can be calculated from the distance between adjacent lines because wave speed $v = f\lambda$. Because the wavelength λ is smaller for the *Ceacam16*$^{\beta gal/\beta gal}$ TM ($\lambda = 380$ μm) than for the wild-type TM ($\lambda = 380$ μm), it follows that the speed is also smaller ($v = 3.80$ m/s for the *Ceacam16*$^{\beta gal/\beta gal}$ TM vs. 4.64 m/s for the wild-type).

Similar results for multiple preparations and for frequencies from 10 to 15 kHz are presented in Fig. 2. Across this range of frequencies, wave speeds (Fig. 2 *A*) for TMs

from adult *Ceacam16*$^{\beta gal/\beta gal}$ mice (*green circles*) tend to be smaller than those from juvenile *Ceacam16*$^{\beta gal/\beta gal}$ mice (*orange Y signs*) and smaller than those from wild-type mice (*blue plus signs*). These trends are summarized in bar plots (Fig. 2 *C*), where the heights of the colored bars represent the median speeds, and the black lines represent interquartile ranges (iqr's).

Wave speeds were generally slower for adult *Ceacam16*$^{\beta gal/\beta gal}$ TMs (median: 4.55 m/s; iqr: 3.68–4.76 m/s; $n = 49$ measurements from five preparations) than for wild-type TMs (median: 5.88 m/s; iqr: 5.12–6.62 m/s; $n = 50$ measurements from six preparations), and the difference was highly significant ($p < 10^{-6}$ in Welch's *t*-test, with $t = 6.55$ and 68.1 (dof), computed using the Satterthwaite approximation (40)). Median wave speeds for young *Ceacam16*$^{\beta gal/\beta gal}$ TMs (median: 5.17 m/s; iqr: 4.50–6.89 m/s; $n = 12$ measurements from two preparations) were between those for adult *Ceacam16*$^{\beta gal/\beta gal}$ TMs and those for wild-type TMs. Differences between young *Ceacam16*$^{\beta gal/\beta gal}$ and adult *Ceacam16*$^{\beta gal/\beta gal}$ TMs ($p < 0.0061$, with $t = 2.92$ and 12.8 dof) were highly significant (i.e., $p < 0.01$). Differences between young *Ceacam16*$^{\beta gal/\beta gal}$ TMs and wild-type TMs were not statistically significant ($p = 0.11$, with $t = 1.28$ and 20.8 dof).

Decay constants for TMs from adult *Ceacam16*$^{\beta gal/\beta gal}$ mice (Fig. 2 *B*, *green circles*) also tend to be smaller than those for juvenile *Ceacam16*$^{\beta gal/\beta gal}$ mice (*orange Y signs*) or those for wild-type mice (*blue plus signs*), and decay constants for TMs from wild-type mice tend to be larger than those for juvenile or adult *Ceacam16*$^{\beta gal/\beta gal}$ mice. These trends are summarized in the bar plots shown in Fig. 2 *D*. Decay constants were generally smaller for adult *Ceacam16*$^{\beta gal/\beta gal}$ TMs (median: 94 μm; iqr: 77–121 μm; $n = 49$ measurements from five preparations) than for wild-type TMs (median: 196 μm; iqr: 164–239 μm; $n = 50$ measurements from six preparations), and the difference was highly significant ($p < 10^{-6}$, with $t = 8.19$ and 96.3 dof). Median decay constants for young *Ceacam16*$^{\beta gal/\beta gal}$ TMs (median: 123 μm; iqr: 91–207 μm; $n = 12$ measurements from two preparations) were between those for adult *Ceacam16*$^{\beta gal/\beta gal}$ TMs and those for wild-type TMs. Decay constants for TMs from juvenile *Ceacam16*$^{\beta gal/\beta gal}$ mice were not significantly different from those for wild-type mice ($p = 0.21$, with $t = 0.83$ and 12.0 dof) or adult *Ceacam16*$^{\beta gal/\beta gal}$ mice ($p = 0.079$, with $t = 1.50$ and 11.9 dof).

In summary, we measured wave parameters of three mouse populations: adult *Ceacam16*$^{\beta gal/\beta gal}$ mice, juvenile *Ceacam16*$^{\beta gal/\beta gal}$ mice, and wild-type mice. Both the wave speeds and decay constants were smaller in adult *Ceacam16*$^{\beta gal/\beta gal}$ TMs than in wild-type TMs, and those differences were highly significant, demonstrating important mechanical differences between *Ceacam16*$^{\beta gal/\beta gal}$ and wild-type TMs. Also, the wave speeds in adult *Ceacam16*$^{\beta gal/\beta gal}$ TMs are smaller than those in juvenile *Ceacam16*$^{\beta gal/\beta gal}$ TMs, and these differences are highly significant, demonstrating age-related changes in the mechanical properties of *Ceacam16*$^{\beta gal/\beta gal}$ TMs.

TM material parameters for *Ceacam16*$^{\beta gal/\beta gal}$ and wild-type TMs

Wave properties of viscoelastic materials derive from their material properties according to the following relationship (41,42):

$$\left(\frac{2\pi}{\lambda} - j\frac{1}{\sigma}\right)^2 = k^2 = \frac{\rho\omega^2}{G' + j\omega\eta}, \tag{3}$$

where ρ is density, G' is shear modulus, η is shear viscosity, and ω is angular frequency in radians/s. We can use this relationship to compute the material properties (G' and η) from the wave properties (λ and σ) presented in the previous section. Notice, however, that these material properties also depend on both density ρ and angular frequency ω. We can account for the dependence on ρ and ω by defining normalized material properties $G'/(\rho\omega^2)$ and $\eta/(\rho\omega)$:

$$\left(\frac{2\pi}{\lambda} - j\frac{1}{\sigma}\right)^2 = k^2 = \frac{1}{\frac{G'}{\rho\omega^2} + j\frac{\eta}{\rho\omega}}, \tag{4}$$

which depend on only λ and σ. In Fig. 3 we illustrate the dependence of normalized shear modulus (Fig. 3 *B*) and normalized shear viscosity (Fig. 3 *C*) on wave parameters. We use these maps to convert the range of observed wave parameters (Fig. 3 *A*) to corresponding ranges of normalized material properties (Fig. 3 *D*) for wild-type and *Ceacam16*$^{\beta gal/\beta gal}$ TMs.

The two-dimensional maps in Fig. 3 *A* provide a concise representation of differences between the wave properties of adult *Ceacam16*$^{\beta gal/\beta gal}$ and wild-type TMs, which have nonoverlapping interquartile ranges in both wavelength and decay constant dimensions. By contrast, the interquartile ranges of these wave properties for juvenile *Ceacam16*$^{\beta gal/\beta gal}$ TMs overlap with both adult *Ceacam16*$^{\beta gal/\beta gal}$ and wild-type TMs. There is considerable overlap of the corresponding material properties in Fig. 3 *D*. The median values of normalized shear viscosity for the TMs of juvenile *Ceacam16*$^{\beta gal/\beta gal}$ and wild-type mice are similar (median: 3.52 $(\mu m)^2$; iqr: 2.33–3.86 $(\mu m)^2$; $n = 12$ measurements from two preparations for the former; median: 3.45 $(\mu m)^2$; iqr: 2.29–5.20 $(\mu m)^2$; $n = 50$ measurements from six preparations for the latter). However, the median value of normalized shear viscosity of adult *Ceacam16*$^{\beta gal/\beta gal}$ TMs (median: 1.90 $(\mu m)^2$; iqr: 1.46–2.36 $(\mu m)^2$; $n = 49$ measurements from five preparations) is smaller than that of juvenile *Ceacam16*$^{\beta gal/\beta gal}$ TMs by a factor of 1.85. The median value of normalized shear modulus for juvenile *Ceacam16*$^{\beta gal/\beta gal}$ TMs (median: 1.89 $(\mu m)^2$; iqr: 0.69–3.73 $(\mu m)^2$; $n = 12$ measurements

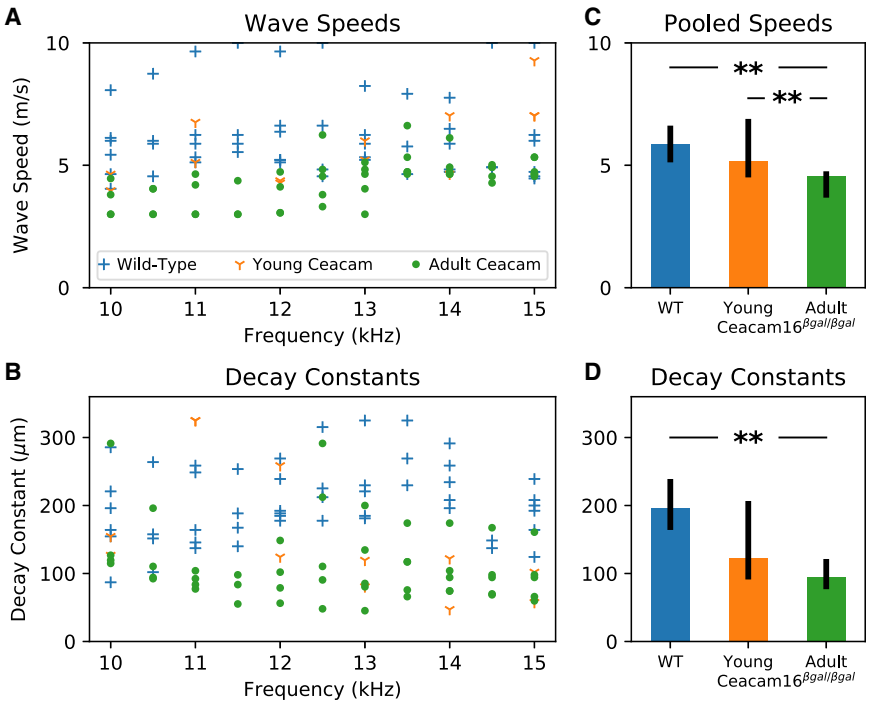

FIGURE 2 Wave properties of TMs from *Ceacam16*$^{+/+}$ and *Ceacam16*$^{\beta gal/\beta gal}$ mice. (*A* and *B*) Wave speed was computed as $v = f\lambda$, where f represents frequency in hertz and λ represents the distance that the wave travels during one cycle of the stimulus. Decay constants represent the distance that the wave travels as its amplitude decays by a factor of e. Results for wild-type and for adult and juvenile *Ceacam16*$^{\beta gal/\beta gal}$ TMs are shown as blue plus signs, green circles, and orange Y signs, respectively. (*C* and *D*) Pooled responses across frequency were characterized by their medians (heights of *colored bars*) and interquartile ranges (*black lines*). Double asterisks (**) indicate pairs of conditions for which the differences are highly significant ($p < 0.01$). To see this figure in color, go online.

from two preparations) is nearly a factor of two smaller than that for wild-type TMs (median: 3.74 $(\mu m)^2$; iqr: 3.07–4.40 $(\mu m)^2$; $n = 50$ measurements from six preparations). The median value of normalized shear modulus for adult *Ceacam16*$^{\beta gal/\beta gal}$ TMs (median: 1.11 $(\mu m)^2$; iqr: 0.66–1.63 $(\mu m)^2$; $n = 49$ measurements from five preparations) is more than three times smaller than that for wild-type TMs.

In summary, the normalized shear moduli of adult *Ceacam16*$^{\beta gal/\beta gal}$ TMs tend to be smaller than those of juvenile *Ceacam16*$^{\beta gal/\beta gal}$ TMs, and those of juvenile *Ceacam16*$^{\beta gal/\beta gal}$ TMs then tend to be smaller than those of wild-type TMs. These trends are consistent with the increasing prominence of holes in the TMs of mice lacking *Ceacam16* (34). However, the normalized shear viscosity of juvenile *Ceacam16*$^{\beta gal/\beta gal}$ TMs is comparable with that of wild-type TMs, suggesting that different mechanisms may contribute shear viscosity and shear stiffness.

Comparisons of properties of *Ceacam16*$^{\beta gal/\beta gal}$, *Tecta*$^{Y1870C/+}$, and *Tectb*$^{-/-}$ TMs

We have previously measured wave and material properties in mice with mutations that target α-tectorin (*Tecta*$^{Y1870C/+}$) and β-tectorin (*Tecta*$^{Y1870C/+}$). Both of these mutations reduce TM shear modulus relative to wild-type TMs (18,43). However, the two mutations are associated with different hearing phenotypes; *Tectb*$^{-/-}$ mice have sharpened basilar membrane tuning by a factor of two to three at mid and high frequencies (13), whereas *Tecta*$^{Y1870C/+}$ mice have normal basilar membrane tuning and even broader neural tuning (11). Because the stiffnesses of *Tecta*$^{Y1870C/+}$ and *Tectb*$^{-/-}$ TMs are similar, stiffness alone cannot account for observed differences in hearing phenotypes. However, there are also differences in viscous loss. The viscous component of *Tecta*$^{Y1870C/+}$ TM shear impedance is approximately a factor of three smaller than that of wild-types (43). In contrast, the shear viscosity of *Tectb*$^{-/-}$ TMs is similar to that of wild-types (18). Paradoxically, the larger viscosity in *Tectb*$^{-/-}$ TMs is associated with sharper tuning, which is the opposite of predictions from conventional models of viscous loss.

Wave and material properties of adult *Ceacam16*$^{\beta gal/\beta gal}$ and wild-type TMs are compared with previously published results for *Tecta*$^{Y1870C/+}$ and *Tectb*$^{-/-}$ TMs (22) in Fig. 4. Decay constants (Fig. 4 *A*) for *Tecta*$^{Y1870C/+}$ TMs (median: 247 μm; iqr: 181–314 μm; $n = 12$ measurements from seven preparations) are generally greater than those for *Tectb*$^{-/-}$ TMs (median: 162 μm; iqr: 121–204 μm; $n = 8$ measurements from four preparations), and those for *Tectb*$^{-/-}$ TMs are generally greater than those for *Ceacam16*$^{\beta gal/\beta gal}$ TMs (median: 94 μm; iqr: 77–121 μm; $n = 49$ measurements from five preparations). Both of these relations are statistically significant ($p = 0.014$, with $t = 2.38$ and 18.0 dof for the former, and $p = 0.029$, with $t = 2.18$ and 8.9 dof for the latter).

Wavelengths for *Tectb*$^{-/-}$ TMs (median: 422 μm; iqr: 370–474 μm; $n = 12$ measurements from four preparations) are generally greater than those for both *Ceacam16*$^{\beta gal/\beta gal}$ TMs (median: 339 μm; iqr: 300–381 μm; $n = 49$ measurements from five preparations) and *Tecta*$^{Y1870C/+}$ TMs (median: 310 μm; iqr: 259–360 μm; $n = 12$ measurements from seven preparations). Both of these relations are highly

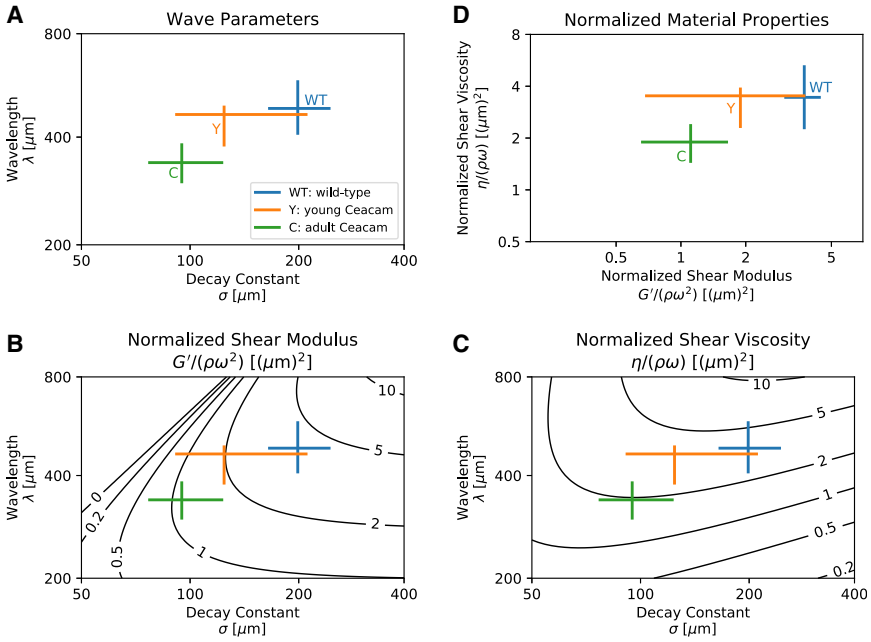

FIGURE 3 Wave parameters and material properties of *Ceacam16*$^{\beta gal/\beta gal}$ and wild-type TMs. (*A*) Wave parameters. Vertical and horizontal line segments represent the interquartile ranges of decay constants σ and wavelengths λ measured for wild-type (WT) and *Ceacam16*$^{\beta gal/\beta gal}$ (adult is represented by *green C*, and young is *orange Y*) TMs. Corresponding vertical and horizontal lines intersect at respective median values. (*B* and *C*) Dependence of normalized shear modulus and normalized shear viscosity on wave parameters. The colored line segments illustrate regions of wave parameter space occupied by WT and *Ceacam16*$^{\beta gal/\beta gal}$ adult (*green C*) and juvenile (*orange Y*) TMs. These regions determine corresponding ranges of normalized shear modulus (*B*) and normalized shear viscosity (*B*). (*D*) Material properties. Vertical and horizontal line segments represent the interquartile ranges of normalized material properties computed from the maps in (*B* and *C*). Corresponding vertical and horizontal lines intersect at respective median values. To see this figure in color, go online.

significant ($p = 0.0021$, with $t = 3.41$ and 14.4 dof for the former; $p = 0.00078$, with $t = 3.61$ and 22.0 dof for the latter). The small differences in wavelengths for *Ceacam16*$^{\beta gal/\beta gal}$ TMs and *Tecta*$^{Y1870C/+}$ TMs are not statistically significant ($p = 0.10$, with $t = 1.33$ and 14.6 dof).

Fig. 4, *B* and *C* illustrate how the preceding wave parameters map to normalized material properties, with the results shown in Fig. 4 *D*. The normalized shear moduli for *Tecta*$^{Y1870C/+}$ (median: 2.16 $(\mu m)^2$; iqr: 1.57–2.80 $(\mu m)^2$; $n = 12$ measurements from seven preparations) and *Tectb*$^{-/-}$ TMs (median: 2.72 $(\mu m)^2$; iqr: 1.81–3.27 $(\mu m)^2$; $n = 8$ measurements from four preparations) are not significantly different ($p = 0.13$, with $t = 1.18$ and 13.4 dof). However, both are smaller than those of wild-type TMs (median: 3.74 $(\mu m)^2$; iqr: 3.07–4.40 $(\mu m)^2$; $n = 50$ measurements from six preparations) and larger than those of adult *Ceacam16*$^{\beta gal/\beta gal}$ TMs (median: 1.11 $(\mu m)^2$; iqr: 0.66–1.63 $(\mu m)^2$; $n = 49$ measurements from five preparations), and these differences are statistically significant ($p = 0.019$, with $t = 2.44$ and 9.0 dof for the comparison of wild-type and *Tectb*$^{-/-}$ TMs, and $p = 0.0014$, with $t = 3.60$ and 14.5 dof for the comparison of *Tecta*$^{Y1870C/+}$ and *Ceacam16*$^{\beta gal/\beta gal}$ TMs).

The normalized shear viscosities of *Tectb*$^{-/-}$ TMs (median: 2.72 $(\mu m)^2$; iqr: 1.96–3.58 $(\mu m)^2$; $n = 8$ measurements from four preparations) and wild-type TMs (median: 3.45 $(\mu m)^2$; iqr: 2.29–5.20 $(\mu m)^2$; $n = 50$ measurements from six preparations) are not significantly different ($p = 0.097$, with $t = 1.35$ and 15.5 dof). But the normalized shear viscosities of *Ceacam16*$^{\beta gal/\beta gal}$ TMs (median: 1.90 $(\mu m)^2$; iqr: 1.46–2.36 $(\mu m)^2$; $n = 49$ measurements from five preparations) tend to be smaller than those of *Tectb*$^{-/-}$ ($p = 0.051$, with $t = 1.85$ and 7.7 dof), and those of *Tecta*$^{Y1870C/+}$ TMs (median: 0.90 $(\mu m)^2$; iqr: 0.54–1.37 $(\mu m)^2$; $n = 12$ measurements from seven preparations) are smaller than those of *Ceacam16*$^{\beta gal/\beta gal}$ TMs ($p < 10^{-4}$, with $t = 4.79$ and 17.8 dof).

Interestingly, the progression from largest to smallest values of normalized shear modulus is different from that for normalized shear viscosity. In particular, the normalized shear modulus of the *Tecta*$^{Y1870C/+}$ TMs was greater than that of the *Ceacam16*$^{\beta gal/\beta gal}$ TMs, whereas the normalized shear viscosity of the *Tecta*$^{Y1870C/+}$ TMs was smaller than that of the *Ceacam16*$^{\beta gal/\beta gal}$ TMs. These results make it clear that the mechanisms that underlie viscosity and stiffness differ.

Implications of differences in material properties

The median value of normalized shear modulus for *Ceacam16*$^{\beta gal/\beta gal}$ TMs is smaller than that of *Tectb*$^{-/-}$ TMs, and both of these are smaller than that of wild-type TMs. The similarity of these trends with those for normalized shear viscosity suggests that both trends may result from a decrease in striated sheet matrix that contributes to both of these material properties. Interestingly, a similar trend does not hold for *Tecta*$^{Y1870C/+}$ TMs. Whereas the median shear modulus for *Ceacam16*$^{\beta gal/\beta gal}$ TMs is approximately half that for *Tecta*$^{Y1870C/+}$ TMs, the median shear viscosity for *Ceacam16*$^{\beta gal/\beta gal}$ TMs is more than a factor of two greater than that for *Tecta*$^{Y1870C/+}$ TMs. This prominent difference suggests that other important structural changes (such as protein cross-linking) are likely to be important

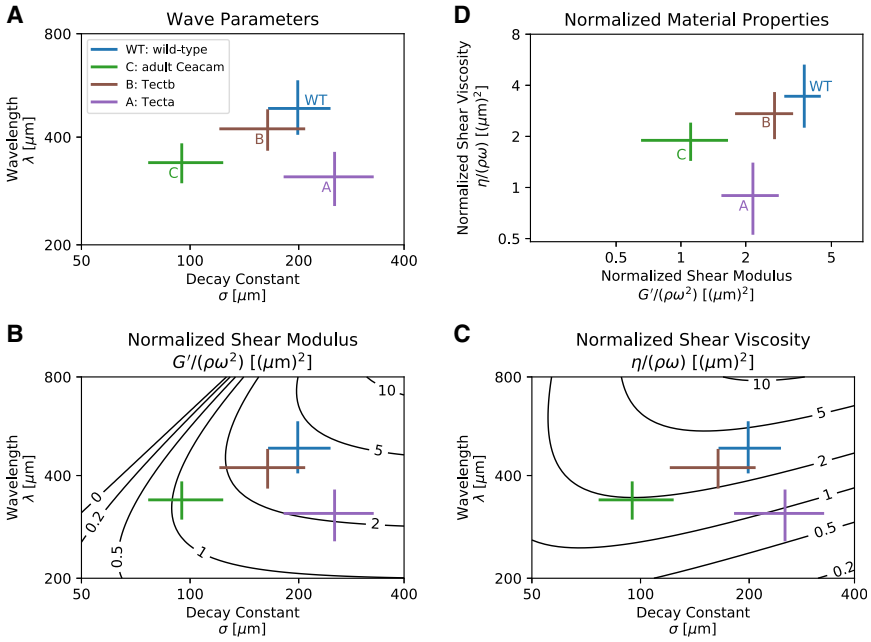

FIGURE 4 Comparison of wave and material properties of *Ceacam16*$^{\beta gal/\beta gal}$, *Tecta*$^{Y1870C/+}$, and *Tectb*$^{-/-}$ TMs. (*A*) Wave parameters for wild-type (WT), *Tecta*$^{Y1870C/+}$ (*A*), *Tectb*$^{-/-}$ (*B*), and adult *Ceacam16*$^{\beta gal/\beta gal}$ (*C*) TMs. (*B* and *C*) Dependence of normalized shear modulus and normalized shear viscosity on wave parameters. (*D*) Material properties of *Ceacam16*$^{\beta gal/\beta gal}$, *Tecta*$^{Y1870C/+}$, and *Tectb*$^{-/-}$ TMs. Other aspects of this figure are described in the caption of Fig. 3. To see this figure in color, go online.

for understanding differences in the shear viscosities of these mutant TMs.

Implications for cochlear mechanisms

The hearing phenotype associated with mice without functional CEACAM16 differs from that associated with wild-type mice in (at least) two important ways: SOAEs are much more prevalent in juvenile *Ceacam16*$^{\beta gal/\beta gal}$ mice than in age-matched wild-types, and adult *Ceacam16*$^{\beta gal/\beta gal}$ mice have progressive elevation of hearing thresholds relative to age-matched wild-types (28,34). The decreases in shear storage modulus and shear viscosity shown in Fig. 3 could play important roles in both of these characteristics of the *Ceacam16*$^{\beta gal/\beta gal}$ phenotype. Recent models (44) suggest that reducing viscous and elastic coupling through the TM increases the prevalence of unstable modes (and presumably the prevalence of SOAEs) and decreases cochlear sensitivity to low-level stimuli.

The median values of normalized shear modulus and normalized shear viscosity progress from 3.74 $(\mu m)^2$ and 3.45 $(\mu m)^2$ for wild-type TMs to 1.89 $(\mu m)^2$ and 3.52 $(\mu m)^2$ for juvenile *Ceacam16*$^{\beta gal/\beta gal}$ TMs to 1.11 $(\mu m)^2$ and 1.90 $(\mu m)^2$ for adult *Ceacam16*$^{\beta gal/\beta gal}$ TMs, corresponding to an average of 0.5, 2, and 30 unstable modes, respectively (44). Whereas this modeling predicts an age-related increase in unstable modes, the reverse is seen in experiments in which SOEs were observed in 70% of juvenile *Ceacam16*$^{\beta gal/\beta gal}$ mice but in only 10% of *Ceacam16*$^{\beta gal/\beta gal}$ mice at 6–7 months of age. Although young mutants retain wild-type-like sensitivity (as assessed with ABR thresholds), they have reduced DPOAEs at 6–7 months of age, as do *Tecta*$^{Y1870C/+}$ mice. In fact, both mutants show a partial loss of gain (as assessed ABR thresholds), yet the *Tecta*$^{Y1870C/+}$ mice are prolific emitters (45), whereas the older mice lacking *Ceacam16* are not.

TM properties other than shear storage modulus (G') and shear viscosity (η) could further complicate these comparisons. Our experimental chamber was designed to observe the longitudinal spread of radial excitation of the TM. However, other modes of motion could also be important given that the TM is morphologically (46) and functionally anisotropic (47–49). For example, it has been suggested that length changes of outer hair cells can induce transverse motions of the subtectorial fluid and the overlying TM, thereby enhancing inner hair cell excitations (16). Longitudinal motions have also been reported (50) and may play a role in creating vibration hotspots (see discussion in (50)). All of these factors point to the importance of considering the three-dimensional nature of mechanical interactions within the cochlear partition.

The anisotropic structure of the TM mirrors its anisotropic architecture, with collagenous proteins contributing to its network of radial fibers coursing through a striated sheet matrix composed primarily of two noncollagenous proteins: α-tectorin (TECTA) and β-tectorin (TECTB) (51). Whereas *Tecta* and *Tectb* are expressed at high levels during development, their expression is not detectable after postnatal day 22 (36). In contrast, *Ceacam16* is expressed from postnatal day 12 into adulthood (32), suggesting that CEACAM16 may stabilize TECTA in the TMs of adults because the two proteins are known to interact (31).

Other mechanical properties may also contribute to changes in hearing associated with *Ceacam16*$^{\beta gal/\beta gal}$

mice. For example, differences in coupling between neighboring outer hair cells, loss of Hensen's stripe, changes in the subtectorial space, and/or the emergence of holes in the TMs of mutant mice could influence the degree to which SOAEs are generated (28,44). Furthermore, the recent demonstration (24) that nanomechanical properties of the TM differ substantially from the micromechanical properties measured in this study may be especially relevant because they predict that mechanical interactions between the TM and individual hair bundles may differ significantly from those that govern longitudinal coupling within the core of the TM. It has also been suggested that the TM may act as a calcium reservoir (52). Given the several calcium-dependent processes that influence the tip-link and transducer complex, the implications of changes to the structure, the material properties, and the wave characteristics of the TM are not yet fully understood.

CONCLUSIONS

CEACAM16 is a noncollagenous glycoprotein that is essential to normal hearing and to the structure of the striated sheet matrix that comprises the core of the TM. Mice that lack *Ceacam16* exhibit an increased incidence of SOAEs as juveniles and progressive hearing loss as adults. To better understand the cochlear mechanisms that underlie these behavioral changes, we have measured wave and material properties of TMs isolated from *Ceacam16*$^{\beta gal/\beta gal}$ and wild-type mice and determined that adult but not juvenile mutants have statistically different wave speeds and decay constants relative to controls. Additionally, we compared those results to previous measurements in *Tecta*$^{Y1870C/+}$ and *Tectb*$^{-/-}$ mutants. Results show a clear separation of wave properties. Interestingly, there is a monotonic progression, with both median wave speed and median decay constants being larger in wild-type TMs than in *Tectb*$^{-/-}$ TMs and larger in *Tectb*$^{-/-}$ TMs than in adult *Ceacam16*$^{\beta gal/\beta gal}$ TMs. However, *Tecta*$^{Y1870C/+}$ TMs do not follow this same monotonic progression; instead, they have significantly slower speeds and larger decay constants than would be expected from the trends for the other groups.

Correlations between these results and previously measured threshold shifts suggest that the slower speeds observed in adult *Ceacam16*$^{\beta gal/\beta gal}$ as well as in *Tecta*$^{Y1870C/+}$ and *Tectb*$^{-/-}$ TMs may contribute to the increase in hearing thresholds, as suggested in some cochlear models (53). Furthermore, whereas relatively small differences in material properties were observed in juvenile *Ceacam16*$^{\beta gal/\beta gal}$ TMs relative to wild-type TMs, recent models (44) show that these differences are sufficient to increase the number of SOAEs in juvenile *Ceacam16*$^{\beta gal/\beta gal}$ TMs. By contrast, the relatively large differences in material properties in adult *Ceacam16*$^{\beta gal/\beta gal}$ TMs would decrease sensitivity (as seen in behavioral tests) and thereby also inhibit SOAEs that would otherwise be even more numerous than in juveniles.

In conclusion, comparisons of *Ceacam16*$^{\beta gal/\beta gal}$, *Tecta*$^{Y1870C/+}$, and *Tectb*$^{-/-}$ TMs suggest that the behavior of the TM is a result of a combination of properties that interact in complicated ways to assure proper hair cell activation and to stabilize the active process. It follows that properties of the hearing phenotype can depend in complicated ways on the many properties of the TM.

AUTHOR CONTRIBUTIONS

J.B.S., A.M., R.G., M.A.C., and D.M.F. designed the research. A.M. and J.B.S. performed the research. A.M., D.F., and J.B.S. analyzed the data. J.B.S., A.M., R.G., M.A.C., and D.M.F. wrote the study.

ACKNOWLEDGMENTS

This work was supported by National Institutes of Health grant R01-DC00238 and R01-DC000089.

REFERENCES

1. Dalhoff, E., D. Turcanu, …, A. W. Gummer. 2007. Distortion product otoacoustic emissions measured as vibration on the eardrum of human subjects. *Proc. Natl. Acad. Sci. USA.* 104:1546–1551.
2. Dallos, P. 1996. Overview: cochlear neurobiology. *In* The Cochlea, Volume 8 of Springer Handbook of Auditory Research. P. Dallos, A. N. Popper, and R. R. Fay, eds. Springer-Verlag.
3. Robles, L., and M. A. Ruggero. 2001. Mechanics of the mammalian cochlea. *Physiol. Rev.* 81:1305–1352.
4. Dallos, P., B. N. Evans, and R. Hallworth. 1991. Nature of the motor element in electrokinetic shape changes of cochlear outer hair cells. *Nature.* 350:155–157.
5. Ashmore, J. 2008. Cochlear outer hair cell motility. *Physiol. Rev.* 88:173–210.
6. Dallos, P. 2008. Cochlear amplification, outer hair cells and prestin. *Curr. Opin. Neurobiol.* 18:370–376.
7. Liberman, M. C., J. Gao, …, J. Zuo. 2002. Prestin is required for electromotility of the outer hair cell and for the cochlear amplifier. *Nature.* 419:300–304.
8. Chan, D. K., and A. J. Hudspeth. 2005. Ca2+ current-driven nonlinear amplification by the mammalian cochlea in vitro. *Nat. Neurosci.* 8:149–155.
9. Fettiplace, R., and C. M. Hackney. 2006. The sensory and motor roles of auditory hair cells. *Nat. Rev. Neurosci.* 7:19–29.
10. Hudspeth, A. J. 2008. Making an effort to listen: mechanical amplification in the ear. *Neuron.* 59:530–545.
11. Legan, P. K., V. A. Lukashkina, …, G. P. Richardson. 2005. A deafness mutation isolates a second role for the tectorial membrane in hearing. *Nat. Neurosci.* 8:1035–1042.
12. Legan, P. K., V. A. Lukashkina, …, G. P. Richardson. 2000. A targeted deletion in α-tectorin reveals that the tectorial membrane is required for the gain and timing of cochlear feedback. *Neuron.* 28:273–285.
13. Russell, I. J., P. K. Legan, …, G. P. Richardson. 2007. Sharpened cochlear tuning in a mouse with a genetically modified tectorial membrane. *Nat. Neurosci.* 10:215–223.
14. Allen, J. B. 1980. Cochlear micromechanics–a physical model of transduction. *J. Acoust. Soc. Am.* 68:1660–1670.
15. Zwislocki, J. J. 1980. Five decades of research on cochlear mechanics. *J. Acoust. Soc. Am.* 67:1679–1685.

16. Nowotny, M., and A. W. Gummer. 2006. Nanomechanics of the subtectorial space caused by electromechanics of cochlear outer hair cells. *Proc. Natl. Acad. Sci. USA.* 103:2120–2125.

17. Ghaffari, R., A. J. Aranyosi, and D. M. Freeman. 2007. Longitudinally propagating traveling waves of the mammalian tectorial membrane. *Proc. Natl. Acad. Sci. USA.* 104:16510–16515.

18. Ghaffari, R., A. J. Aranyosi, …, D. M. Freeman. 2010. Tectorial membrane travelling waves underlie abnormal hearing in Tectb mutant mice. *Nat. Commun.* 1:96.

19. Meaud, J., and K. Grosh. 2010. The effect of tectorial membrane and basilar membrane longitudinal coupling in cochlear mechanics. *J. Acoust. Soc. Am.* 127:1411–1421.

20. Lee, H. Y., P. D. Raphael, …, J. S. Oghalai. 2015. Noninvasive in vivo imaging reveals differences between tectorial membrane and basilar membrane traveling waves in the mouse cochlea. *Proc. Natl. Acad. Sci. USA.* 112:3128–3133.

21. Jones, G. P., V. A. Lukashkina, …, A. N. Lukashkin. 2013. Frequency-dependent properties of the tectorial membrane facilitate energy transmission and amplification in the cochlea. *Biophys. J.* 104:1357–1366.

22. Sellon, J. B., R. Ghaffari, …, D. M. Freeman. 2014. Porosity controls spread of excitation in tectorial membrane traveling waves. *Biophys. J.* 106:1406–1413.

23. Sellon, J. B., S. Farrahi, …, D. M. Freeman. 2015. Longitudinal spread of mechanical excitation through tectorial membrane traveling waves. *Proc. Natl. Acad. Sci. USA.* 112:12968–12973.

24. Sellon, J. B., M. Azadi, …, D. M. Freeman. 2019. Nanoscale poroelasticity of the tectorial membrane determines hair bundle deflections. *Phys. Rev. Lett.* 122:028101.

25. Steel, K. P. 2000. A take on the tectorial membrane. *Nat. Genet.* 24:104.

26. Verhoeven, K., L. Van Laer, …, G. Van Camp. 1998. Mutations in the human alpha-tectorin gene cause autosomal dominant non-syndromic hearing impairment. *Nat. Genet.* 19:60–62.

27. Lukashkin, A. N., P. K. Legan, …, G. P. Richardson. 2012. A mouse model for human deafness DFNB22 reveals that hearing impairment is due to a loss of inner hair cell stimulation. *Proc. Natl. Acad. Sci. USA.* 109:19351–19356.

28. Cheatham, M. A., R. J. Goodyear, …, G. P. Richardson. 2014. Loss of the tectorial membrane protein CEACAM16 enhances spontaneous, stimulus-frequency, and transiently evoked otoacoustic emissions. *J. Neurosci.* 34:10325–10338.

29. Zhang, D.-S., V. Piazza, …, C. P. Lechene. 2012. Multi-isotope imaging mass spectrometry reveals slow protein turnover in hair-cell stereocilia. *Nature.* 481:520–524.

30. Hasko, J. A., and G. P. Richardson. 1988. The ultrastructural organization and properties of the mouse tectorial membrane matrix. *Hear. Res.* 35:21–38.

31. Zheng, J., K. K. Miller, …, P. Dallos. 2011. Carcinoembryonic antigen-related cell adhesion molecule 16 interacts with α-tectorin and is mutated in autosomal dominant hearing loss (DFNA4). *Proc. Natl. Acad. Sci. USA.* 108:4218–4223.

32. Kammerer, R., L. Rüttiger, …, W. Zimmermann. 2012. Loss of mammal-specific tectorial membrane component carcinoembryonic antigen cell adhesion molecule 16 (CEACAM16) leads to hearing impairment at low and high frequencies. *J. Biol. Chem.* 287:21584–21598.

33. Goodyear, R. J., and G. P. Richardson. 2018. Structure, function, and development of the tectorial membrane: an extracellular matrix essential for hearing. *In* Extracellular Matrix and Egg Coats. E. S. Litscher and P. M. Wassarman, eds. Academic Press, pp. 217–244. https://doi.org/10.1016/bs.ctdb.2018.02.006.

34. Goodyear, R. J., M. A. Cheatham, …, G. P. Richardson. 2019. Accelerated age-related degradation of the tectorial membrane in the *Cea-cam16*$^{\beta gal/\beta gal}$ null mutant mouse, a model for late-onset human hereditary deafness DFNB113. *Front. Mol. Neurosci.* 12:147.

35. Goodyear, R. J., X. Lu, …, G. P. Richardson. 2017. A tectorin-based matrix and planar cell polarity genes are required for normal collagen-fibril orientation in the developing tectorial membrane. *Development.* 144:3978–3989.

36. Rau, A., P. K. Legan, and G. P. Richardson. 1999. Tectorin mRNA expression is spatially and temporally restricted during mouse inner ear development. *J. Comp. Neurol.* 405:271–280.

37. Shah, D. M., D. M. Freeman, and T. F. Weiss. 1995. The osmotic response of the isolated, unfixed mouse tectorial membrane to isosmotic solutions: effect of Na+, K+, and Ca2+ concentration. *Hear. Res.* 87:187–207.

38. Horn, B. K., and B. G. Schunck. 1981. Determining optical flow. *In* Proceedings of SPIE 0281, Techniques and Applications of Image Understanding. J. J. Pearson, ed. SPIE, pp. 185–203.

39. Davis, C. Q., and D. M. Freeman. 1998. Statistics of subpixel registration algorithms based on spatio-temporal gradients or block matching. *Opt. Eng.* 37:1290–1298.

40. Satterthwaite, F. E. 1946. An approximate distribution of estimates of variance components. *Biometrics.* 2:110–114.

41. Sellon, J. B., R. Ghaffari, and D. M. Freeman. 2017. Geometric requirements for tectorial membrane traveling waves in the presence of cochlear loads. *Biophys. J.* 112:1059–1062.

42. Greenleaf, J. F., M. Fatemi, and M. Insana. 2003. Selected methods for imaging elastic properties of biological tissues. *Annu. Rev. Biomed. Eng.* 5:57–78.

43. Masaki, K., R. Ghaffari, …, A. J. Aranyosi. 2010. Tectorial membrane material properties in Tecta(Y)(1870C/+) heterozygous mice. *Biophys. J.* 99:3274–3281.

44. Bowling, T., C. Lemons, and J. Meaud. 2019. Reducing tectorial membrane viscoelasticity enhances spontaneous otoacoustic emissions and compromises the detection of low level sound. *Sci. Rep.* 9:7494.

45. Cheatham, M. A., Y. Zhou, …, G. P. Richardson. 2018. Spontaneous otoacoustic emissions in *Tecta*$^{Y1870C/+}$ mice reflect changes in cochlear amplification and how it is controlled by the tectorial membrane. *eNeuro.* 5:2018.

46. Lim, D. J. 1972. Fine morphology of the tectorial membrane. Its relationship to the organ of Corti. *Arch. Otolaryngol.* 96:199–215.

47. Abnet, C. C., and D. M. Freeman. 2000. Deformations of the isolated mouse tectorial membrane produced by oscillatory forces. *Hear. Res.* 144:29–46.

48. Gavara, N., and R. S. Chadwick. 2009. Collagen-based mechanical anisotropy of the tectorial membrane: implications for inter-row coupling of outer hair cell bundles. *PLoS One.* 4:e4877.

49. Masaki, K., J. W. Gu, …, A. J. Aranyosi. 2009. Col11a2 deletion reveals the molecular basis for tectorial membrane mechanical anisotropy. *Biophys. J.* 96:4717–4724.

50. Cooper, N. P., A. Vavakou, and M. van der Heijden. 2018. Vibration hotspots reveal longitudinal funneling of sound-evoked motion in the mammalian cochlea. *Nat. Commun.* 9:3054.

51. Legan, P. K., A. Rau, …, G. P. Richardson. 1997. The mouse tectorins. Modular matrix proteins of the inner ear homologous to components of the sperm-egg adhesion system. *J. Biol. Chem.* 272:8791–8801.

52. Strimbu, C. E., S. Prasad, …, A. Fridberger. 2019. Control of hearing sensitivity by tectorial membrane calcium. *Proc. Natl. Acad. Sci. USA.* 116:5756–5764.

53. Hubbard, A. 1993. A traveling-wave amplifier model of the cochlea. *Science.* 259:68–71.